Optical spectroscopy and crystal-field analysis of U^{3+} : Ba_2YCl_7

Mirosław Karbowiak,[a] Agnieszka Mech,[a] Janusz Drożdżyński,[a] Zbigniew Gajek[b] and Norman M. Edelstein[c]

[a] *Faculty of Chemistry, University of Wrocław, ul. Joliot-Curie 14, 50-383 Wrocław, Poland. E-mail: jd@wchuwr.chem.uni.wroc.pl*
[b] *W.Trzebiatowski Institute of Low Temperature and Structure Research, Polish Academy of Sciences, P. O. Box 1410, 50-950, Wrocław 2, Poland*
[c] *Chemical Sciences Division, MS 70A-1150, Lawrence Berkeley National Laboratory, Berkeley CA 94720, USA*

Received (in Strasbourg, France) 7th March 2002, Accepted 9th August 2002
First published as an Advance Article on the web 18th October 2002

High resolution absorption spectra of a $U^{3+}(0.3\%):Ba_2YCl_7$ single crystal were recorded in the 4000–50 000 cm^{-1} range at 7 K. The observed crystal-field levels were assigned and fit to the parameters of the simplified angular overlap model (AOM) as well as a semi-empirical Hamiltonian representing the combined atomic and one-electron crystal-field interactions. The starting values of the AOM parameters were obtained from *ab intio* calculations. The analysis of the spectra allowed the assignment of 65 crystal-field levels with a relatively small rms deviation of 25 cm^{-1} and has shown that the AOM approach can predict quite well the B_q^k crystal-field parameters. The value determined for the crystal-field strength parameter, N_v, corresponds well with those determined for U^{3+} in other chloride single crystals.

In recent years we have reported the results of crystal-field analyses for U^{3+} doped RbY_2Cl_7,[1] K_2UX_5 (X = Cl, Br or I),[2] Cs_2NaYCl_6[3] and Cs_2LiYCl_6[3] single crystals as well as for some polycrystalline samples.[4–6] Since, in all these chloride crystals, the U^{3+} ions readily undergo hydrolysis and oxidation in the presence of traces of water, we have searched for moisture resistant crystals. To date only fluoride hosts provide such properties. However, due to experimental difficulties, no high quality U^{3+} doped single crystals of a fluoride compound could be grown. Simoni *et al.* have converted U^{4+} ions doped in $LiYF_4$ single crystals into U^{3+} ions by γ-irradiation.[7] This method, however, inevitably leads to a number of site defects. Another important disadvantage is that only a very small UF_4 concentration could be reduced to the U^{3+} state. Since Wickleder *et al.*[8] synthesized, in a systematic search for new host lattices, a series of relatively air-stable Ba_2MCl_7 type of compounds (where M = Gd–Yb, Y) and determined their crystal structure, we turned our attention towards the relatively moisture-stable Ba_2YCl_7 crystal.

Ba_2YCl_7 crystallizes in the monoclinic space group $P2_1/c$ (No. 14).[8] The Y^{3+} ions are seven-coordinated and the characteristic feature of the crystal structure is the [YCl_7] polyhedra, build in the form of a trigonal prism and capped on one rectangular face. Due to a slight distortion of the polyhedra, the Y^{3+} site symmetry is C_1. The [YCl_7] units are isolated with an extremely long Y^{3+}–Y^{3+} distance of approximately 6.5 Å. The Y–Cl distances, approximately 2.7 Å, are typical for yttrium complex chlorides.

In this paper the absorption and emission spectra for U^{3+} : Ba_2YCl_7 are presented and discussed. A crystal-field analysis, based on both the angular overlap model (AOM) and the conventional parametric Hamiltonian, is presented.

Experimental

The starting materials for the synthesis of U^{3+} : Ba_2YCl_7 crystals were $BaCl_2$, YCl_3 and Ba_2UCl_7. Barium dichloride was obtained from $BaCO_3$ by dissolution in concentrated HCl and evaporating the solution to dryness. The product was initially dried in a desiccator under P_2O_5 and finally by heating in vacuum at 400 °C. YCl_3 was prepared from Y_2O_3 (99.99%) following the ammonium halide route. For purification, YCl_3 was sublimed in vacuum and passed through a Bridgman furnace. Ba_2UCl_7 was prepared from $BaCl_2$ and UCl_3 as described earlier.[9] Due to incongruent melting,[10] the non-stoichiometric mixture of $BaCl_2$ and 5% excess of YCl_3 was sealed under vacuum in a silica ampoule and passed through a vertical Bridgman–Stockbarger furnace. The Ba_2YCl_7 crystals thus obtained were mixed with Ba_2UCl_7 plus a 5% excess of YCl_3 and the mixture was again passed through the furnace. The nominal doping concentration was 0.3 mole %. The crystals obtained were checked by X-ray powder diffraction. The bulk crystals of 10 mm length and 6 mm in diameter were cut into $\sim 5 \times 5 \times 0.3$ mm plates and polished under dry paraffin oil.

For low temperature absorption and luminescence measurements the crystals were mounted in a low temperature Oxford Instruments model CF1204 optical cryostat and cooled to ~7 K. Unpolarized absorption spectra were recorded on a Cary 5 NIR-Vis-UV spectrophotometer in the 4000–50 000 cm^{-1} range. Excitation and fluorescence spectra were recorded using a Spectra Physics model PDL-3 dye laser with Rhodamine 590 and DCM pumped by the second-harmonic output of a Spectra Physics model GCR-3 Nd : YAG laser. Fluorescence was analyzed using a Spex model 1403 double-grating monochrometer and detected by a thermoelectrically cooled Hamamatsu R943-02 photomultiplier tube. The signal was amplified by a Stanford Research model SR445 fast preamplifier and measured using a Stanford Research model SR250 time gated integrator. Fluorescence transients were recorded using a LeCroy model 9360 digital storage oscilloscope and fitted to a single exponential function to obtain the fluorescence lifetimes of the emitting states. For such low symmetry crystals no information could be drawn from polarized

measurements so the orientation of crystals during absorption and emission measurements was random.

Phenomenological model describing the electronic transitions

Energy-level calculations were carried out by applying the phenomenological model based on the effective Hamiltonian approach.[11–13] The eigenvectors and eigenvalues of the crystal-field levels in this model were obtained by simultaneous diagonalization of the combined free-ion and crystal-field energy matrices. The complete Hamiltonian includes the following terms:

$$\hat{H} = \hat{H}_A + \hat{H}_{CF} \quad (1)$$

$\hat{H}_A$ contains the spherically symmetric (atomic) parts of $\hat{H}$ and is defined as:

$$\hat{H}_A = E_{\text{ave}} + \sum_{k=0,2,4,6} F^k(nf,nf)\hat{f}_k + \zeta_{5f}\hat{A}_{SO} + \alpha\hat{L}(\hat{L}+1) + \beta\hat{G}(G_2) + \gamma\hat{R}(R_7) + \sum_{i=2,3,4,6,7,8} T^i\hat{t}_i + \sum_j M^j\hat{m}_j + \sum_k P^k\hat{p}_k \quad (2)$$

where E_{ave} is the spherically symmetric one-electron part of the Hamiltonian, $F^k(nf, nf)$ and ζ_{5f} represent the radial integrals of the electrostatic and spin-orbit interactions, while f_k and A_{SO} are the angular operators corresponding to these interactions, respectively. The parameters α, β and γ are associated with the two-body correction terms. $G(G_2)$ and $G(R_7)$ are Casimir operators for the G_2 and R_7 groups. L is the total orbital angular momentum. The three-particle configuration interaction is expressed by $T^i t_i$ ($i = 2, 3, 4, 6, 7, 8$), where T^i are parameters and t_i are three-particle operators. The electrostatically correlated spin-orbit perturbation is represented by the P^k parameters and those of the spin-spin and spin-other-orbit relativistic corrections by the M^j parameters. The operators associated with these parameters are designated by m_j and p_k, respectively. The $\hat{H}_{CF}$ term of the Hamiltonian represents the one-electron crystal-field interactions and is defined as:[11,14]

$$\hat{H}_{CF} = \sum_i \left\{ B_0^k \hat{C}_0^{(k)}(i) + \sum_{q=1}^{k} [\text{Re}\, B_q^k (\hat{C}_q^{(k)}(i) + (-1)^q \hat{C}_{-q}^{(k)}(i)) + \text{Im}\, B_q^k i(\hat{C}_q^{(k)}(i) - (-1)^q \hat{C}_{-q}^{(k)}(i))] \right\} \quad (3)$$

where $\hat{C}_q^{(k)}(i)$ is a spherical tensor operator of rank k while B_q^k are crystal-field parameters. For the C_1 symmetry the crystal-field Hamiltonian includes 27 $\text{Re}\, B_q^k$ and $\text{Im}\, B_q^k$ parameters (see Table 1 below). In the fitting procedure the full (364×364) $SLJM_J$ matrix was diagonalized. The calculations have been performed by applying the f-shell empirical programs written by M. Reid[15] and running on a PC under the Linux Mandrake operating system.

Results and discussion

The U^{3+} : Ba_2YCl_7 crystals were clear, with a dark red color characteristic for U^{3+} complex chlorides. In all crystals, however, we have found some features due to U^{4+} ions. In the absorption spectra, the lines attributed to the U^{4+} ion were mostly very weak or not observed. In a number of crystal growth processes we had already observed some conversion of U^{3+} into U^{4+} as well as U^{4+} to U^{3+}. For example, in UCl_4 doped RbY_2Cl_7 or Cs_2NaYCl_6 single crystals, the uranium(IV) ions were to a large extent converted to the tervalent state. This might have resulted from the charge compensation necessary for the substitution of Y^{3+} by U^{4+} ions. We have not observed the appearance of U^{3+} ions in UBr_4 doped $CsCdBr_3$ single crystals. In this case the charge compensation of the U^{4+} ions seemed to be readily performed by two cadmium ions.

Absorption spectra

The absorption spectrum recorded at 7 K is presented in Fig. 1 and 2. In the 4000–15 500 cm^{-1} range the spectrum consists of sharp and well separated absorption bands that arise from intraconfigurational $5f^3 \rightarrow 5f^3$ transitions from the lowest Stark component of the $^4I_{9/2}$ ground multiplet to excited states of $^{2S+1}L_J$ multiplets. Above this spectral range these transitions are obscured by strong and broad $5f^3 \rightarrow 5f^2 6d^1$ bands. Since the origin of all observed bands in this region is not certain we have not include them in the crystal-field energy level calculations. Fig. 3 presents a higher resolution spectrum of transitions to the $^2H_{9/2}$ and $^4F_{5/2}$ multiplets. The number of observed lines is equal to $(2J + 1)/2$, which is indicative of single uranium sites in the crystal. Due to the low site symmetry all levels are non-degenerate, except for Kramer's degeneracy.

The seven intense absorption bands observed in the 8000–8700 cm^{-1} region (Fig. 4) may be readily assigned to transitions to the $^4I_{13/2}$ multiplet. The presence of traces of U^{4+} ions in the crystal seems to be responsible for the appearance of additional weak lines. Fortunately they are weak, do not overlap with the U^{3+} bands and thus do not hamper the analysis. However, the spectrum is not as clear and unmistakable in the other regions.

In the 14 300–15 100 cm^{-1} range [Fig. 5(a)] the observed bands should arise from transitions to the $^4F_{9/2}$ multiplet. In this region, however, the U^{4+} bands seem to be of similar intensities as those of U^{3+}. For proper identification we have utilized time-resolved site-selective laser spectroscopy. The results are presented in the next section.

Due to the low site symmetry vibronic bands were not observed, except for two small lines in the $4I_{9/2} \rightarrow {}^4G_{7/2}$ transition range (Fig. 6) that are assigned as vibronic sidebands. The observed shift from the main electronic lines of 256 cm^{-1} is in accord with the value determined from emission spectra (see next section).

Emission spectra

Excitation of the f–d bands of the U^{3+} ions in Ba_2YCl_7 resulted in emission from the $^4F_{9/2}$ and $^4G_{7/2}$ levels. From an analysis of emission spectra of other U^{3+} doped crystals, a somewhat stronger emission from the $^4F_{3/2}$ (at about 7000 cm^{-1}) and the $^4I_{9/2}$ (about 4300 cm^{-1}) multiplets was expected, but this spectral range was beyond the detection limit of our photomultiplier.

Fig. 7 presents the emission spectrum recorded at 7 K, after 581.5 nm (17197 cm^{-1}) excitation. The five bands of electronic

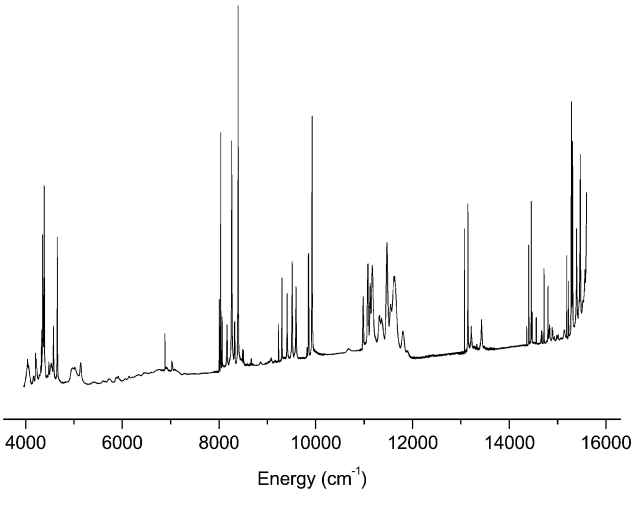

Fig. 1 Unpolarized overview absorption spectrum (4000–15 500 cm^{-1}) of Ba_2YCl_7 : 0.3% U^{3+} at 7 K.

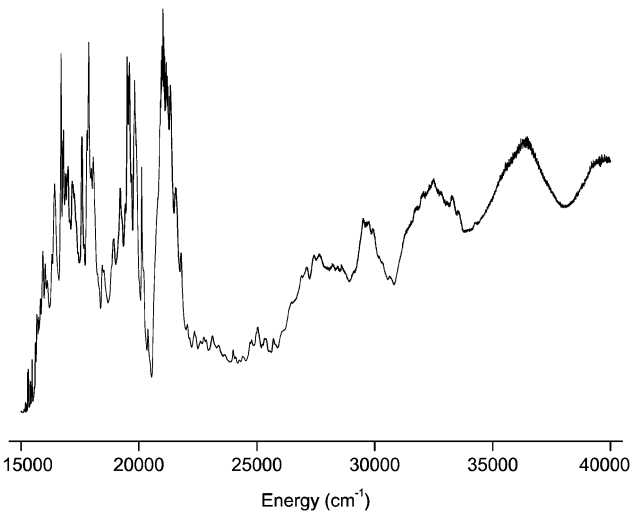

Fig. 2 Unpolarized overview absorption spectrum (15 000–40 000 cm^{-1}) of Ba_2YCl_7 : 0.3% U^{3+} at 7 K.

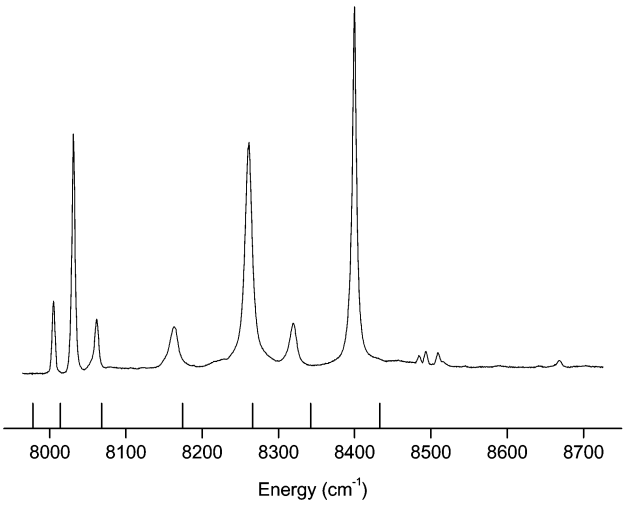

Fig. 4 A detailed view of the $^4I_{9/2} \rightarrow {}^4I_{13/2}$ absorption transitions at 7 K. The bars at the bottom indicate the corresponding values of the calculated crystal-field levels.

origin marked with arrows correspond to transitions from the lowest level of the $^4G_{7/2}$ multiplet to the five Stark's components of the ground $^4I_{9/2}$ multiplet. Some vibrational sidebands, labeled with v_i can be readily identified. They are observed at an energy of 203 (v_i) and 256 (v_i') cm^{-1} from the zero-phonon lines.

The energies of the crystal–field levels of the ground $^4I_{9/2}$ multiplet have been determined from the emission spectra. The overall splitting of 538 cm^{-1} is comparable with the 473 and 567 cm^{-1} values determined for U^{3+} ions in two intrinsic sites, U(1) and U(2), of the U^{3+} : RbY_2Cl_7[1] crystal for which, similarly as for Ba_2YCl_7, the [Y(U)Cl_7] polyhedra are a characteristic structural feature.

The emission from the $^4F_{9/2}$ and $^4G_{7/2}$ levels is quenched at temperatures higher then ~150 K. Fig. 8 presents the 7 K decay curve of the $^4F_{9/2} \rightarrow {}^4I_{9/2}$ emission recorded after excitation of the $^4I_{9/2} \rightarrow {}^4F_{9/2}$ (14 715 cm^{-1}) absorption line. This decay was fitted with two-exponential functions, which resulted in $\tau_1 = 0.53(\pm0.01)$ μs and $\tau_2 = 5.4(\pm0.2)$ μs. The first value is the fluorescence lifetime of the U^{3+} ions. It corresponds well to the 0.94 and 0.23 μs values determined for the U(1) and U(2) sites of the U^{3+} : RbY_2Cl_7 crystal, respectively. The observed longer component on of the decay curve is most probably due to an energy transfer from U^{4+} ions. The lifetime of the U^{4+} emission in Ba_2YCl_7 crystals was determined to be ~10 μs. The processes of energy transfer between U^{3+} and U^{4+} are under investigation and will be presented in a future paper.[16]

On the basis of the luminescence spectrum we have recorded laser site-selective excitation spectra in order to identify the U^{3+} lines in the $^4I_{9/2} \rightarrow {}^4F_{9/2}$ absorption range. For this purpose the 13 821 cm^{-1} emission line, assigned to the $^4F_{9/2} \rightarrow {}^4I_{9/2}$ transition of U^{3+}, was monitored while the absorption region was scanned with laser excitation. The

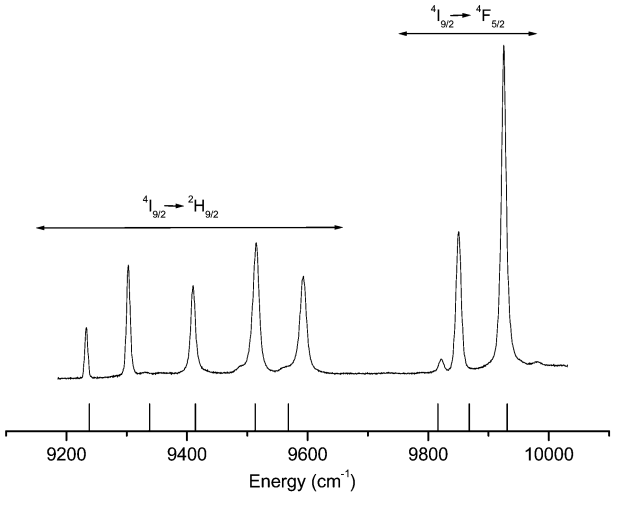

Fig. 3 A detailed view of the $^4I_{9/2} \rightarrow {}^2H_{9/2}$ and $^4I_{9/2} \rightarrow {}^4F_{9/2}$ absorption transitions at 7 K. The bars at the bottom indicate the corresponding values of the calculated crystal-field levels.

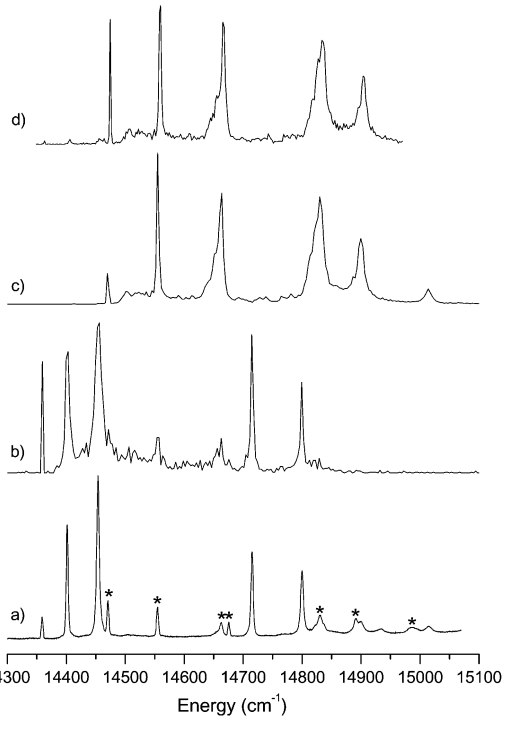

Fig. 5 (a) The 7 K absorption spectrum of U^{3+} in the $^4I_{9/2} \rightarrow {}^4F_{9/2}$ transition range. Lines due to the presence of the U^{4+} impurities are also noticeable and are marked by asterisks. (b) The 7 K excitation spectrum recorded while monitoring the U^{3+} emission line at 13 821 cm^{-1} recorded with 0.5 μs gate delay and 4 μs gate width (c) The 7 K excitation spectrum recorded while monitoring the emission line at 13 961 cm^{-1} assigned to U^{4+} ions. (d) Analogous to spectrum (b) but recorded with 3.5 μs gate delay and 50 μs gate width.

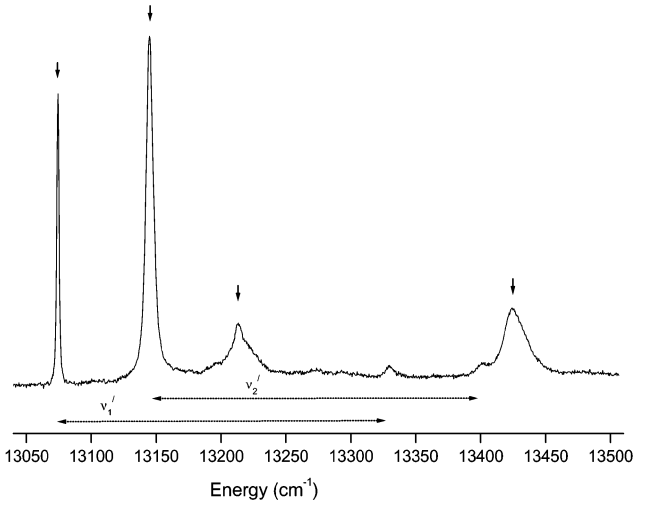

Fig. 6 The 7 K absorption spectrum recorded in the $^4I_{9/2} \rightarrow {}^4G_{7/2}$ spectral range. The two weak vibronic sidebands are shifted from the electronic lines (marked with arrows) by $v_i' = 256$ cm^{-1}.

resulting excitation spectrum is presented in Fig. 5(b). A similar spectrum is shown on in Fig. 5(c), but recorded while monitoring the line at 13 961 cm^{-1}, assigned to U^{4+}[16]. In this way all lines belonging to U^{4+} could be assigned. Since uranium ions in various valence states exhibit considerably different emissions decay times, one may also obtain these assignments by utilizing the temporal resolution of our photon counting system. In Fig. 5(d) an analogous spectrum to that of Fig. 5(b) is shown. The only difference is that in the first case the gate of the photon counter was open 0.5 μs after the laser pulse, while the second spectrum was recorded with a gate delay of 3.5 μs. Thus, the short-lived emission of U^{3+} ions has already decayed and the recorded spectrum is characteristic of the U^{4+} ions and corresponds to that of Fig. 5(c).

Crystal-field (CF) energy level calculations

In the calculations five energy levels of the ground multiplet were included, which were determined from emission measurements, as well as 60 lines assigned in the 4328–16 427 cm^{-1} range from absorption spectra. Most of the sharp lines superimposed on the broad f-d bands above this absorption range

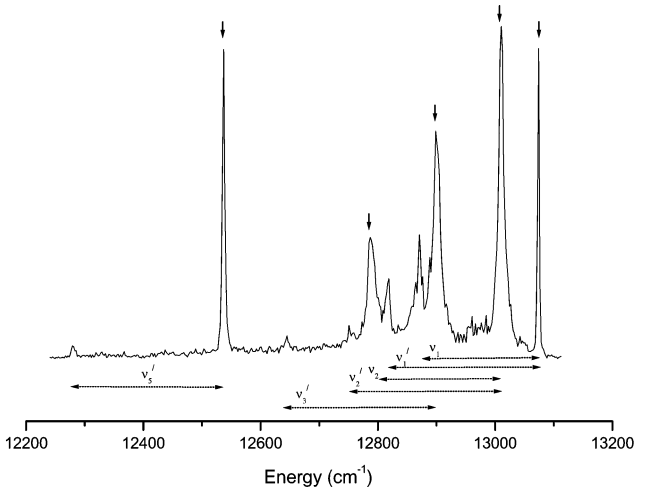

Fig. 7 The 7 K emission spectrum showing the $^4G_{7/2} \rightarrow {}^4I_{9/2}$ transitions of U^{3+} in Ba_2YCl_7, recorded after 581.5 nm excitation. The vibronic sidebands are shifted by $v_i = 203$ cm^{-1} and $v_i' = 256$ cm^{-1} from the ith line of electronic origin. The zero-phonon lines are indicated by arrows.

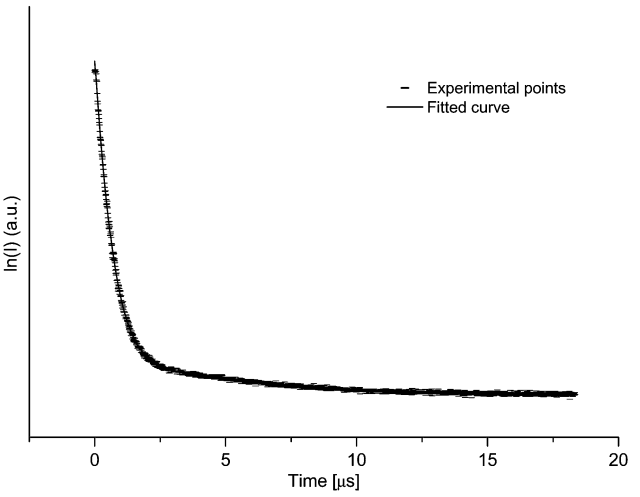

Fig. 8 The decay of the $^4F_{9/2} \rightarrow {}^4I_{9/2}$ emission recorded at 7 K while pumping the $^4I_{9/2} \rightarrow {}^4F_{9/2}$ (14 715 cm^{-1}) absorption line.

are most probably f-f transitions too. Since their assignments may be ambiguous we have not included them in the fitting procedure.

In the first step of the calculations we have taken into account only those crystal-field levels that could be unambiguously assigned to a $S'L'J'$ multiplet; This corresponds to all crystal-field levels in the 0–10 000 cm^{-1} and 12 000–15 000 cm^{-1} spectral ranges. These 41 experimental levels have been marked with an asterik in Table 1. The remaining levels were gradually identified and included into the fitting procedure as the calculation proceeded.

Since, due to the low site symmetry of the U^{3+} ions in the crystal, one cannot obtain additional information for assignments from polarization measurements the identification of the experimental crystal-field levels, the levels of a particular multiplet were assigned to the calculated ones in accordance with increasing energies. In the case where the number of levels was smaller than that predicted by theory, the experimental levels were assigned to the nearest calculated value.

So far, to the best of our knowledge, no CF calculations have been performed for any f-electron ion in this host crystal. Thus, due to the absence of literature data for initial values of CF parameters which could be utilized in our analysis, we started with those obtained from *ab initio* calculations. We applied a perturbation approach comprising leading terms of direct electrostatic, exchange, multipole polarization, and inter-ionic renormalization contributions. This type of calculation has already been employed, among others, in our previous papers.[2,5,6] The details of the method and a discussion of its reliability can be found elsewhere.[14,17–20]

Due to the lack of symmetry at the U^{3+} site in the Ba_2YCl_7 crystal as many as 27 independent, real and imaginary parameters describe the CF potential. A least-squares procedure with so many parameters may lead to a false minimum with no physical meaning. In order to reduce the space of possible solutions we have applied one of the commonly accepted simplified phenomenological CF models, the angular overlap model (AOM), known to be especially efficient in cases of low symmetry systems.[5,6,19] The whole CF effect is described in this approximation by only three AOM parameters: e_σ, e_π and e_δ. Moreover, due to the well-established properties of these AOM parameters further approximations are acceptable.[19,14] In particular, the e_π value can be set to be a fraction of the most important e_σ parameter, which is characteristic for a given metal-ligand bond. In addition, the delta contribution can be entirely neglected: $e_\delta = 0$. Thus, within this special limit e_σ becomes the only independent parameter representing the crystal field potential.

Table 1 Calculated and experimental energy levels for $Ba_2YCl_7 : U^{3+}$

$^{2S+1}L_J$[a]	Calcd energy/ cm^{-1}	Exptal energy/ cm^{-1}	$E_{exp} - E_{calc}$/ cm^{-1}
$^4I_{9/2}$	−8	0*	8
	68	65*	−3
	189	175*	−14
	286	288*	2
	490	538*	48
$^4I_{11/2}$	4314	4328*	14
	4343	4353*	10
	4390	4385*	−5
	4483	4481*	−2
	4567	4577*	10
	4666	4636*	−30
$^4F_{3/2}$	6900	6882*	−18
	7050	7025*	−25
$^4I_{13/2}$	7978	8005*	27
	8014	8031*	17
	8068	8061*	−7
	8174	8164*	−10
	8266	8262*	−4
	8342	8320*	−22
	8433	8400*	−33
$^2H_{9/2}$	9238	9233*	−5
	9388	9303*	−35
	9414	9410*	−4
	9513	9515*	2
	9568	9593*	25
$^4F_{5/2}$	9816	9822*	6
	9868	9851*	−17
	9931	9925*	−6
$^4I_{15/2} + {}^4S_{3/2} + {}^4G_{5/2} + {}^4F_{7/2}$	10 663	10 699	6
	10 969	10 979	10
	11 043	11 074	31
	11 114	11 122	8
	11 171	11 166	5
	11 245	–	–
	11 293	11 315	22
	11 353	11 358	5
	11 413	–	–
	11 487	11 468	−19
	11 542	11 547	5
	11 589	–	–
	11 620	11 627	7
	11 682	–	–
	11 816	11 807	−9
	11 887	11 903	16
	11 983	–	–
$^4G_{7/2}$	13 077	13 074*	−3
	13 156	13 145*	−11
	13 254	13 213*	−41
	13 392	13 426*	34
$^4F_{9/2}$	14 371	14 359*	−12
	14 425	14 402*	−23
	14 502	14 454*	−48
	14 662	14 715*	53
	14 757	14 800*	43
$^2H_{11/2}$	15 161	15 192	31
	15 221	15 231	10
	15 269	15 286	17
	15 347	15 310	−37
	15 417	15 396	−21
	15 465	15 471	6
$^4D_{1/2} + {}^4D_{3/2} + {}^2K_{13/2}$	15 617	15 608	−9
	15 671	15 673	2
	15 738	15 749	11
	15 778	15 785	7
	15 818	15 827	9
	15 937	15 929	−8
	16 016	16 027	11
	16 129	16 109	−20
	16 299	16 307	8
	16 429	16 427	−2

[a] Nominal quantum numbers for the atomic state(s) associated with the group.

The fitting procedure was divided into a number of steps. As the fitting procedure proceeded the initial constraints on the initial single-parameter of the AOM approximation, described above, were subsequently relaxed up to the complete one-electron CF parameterization in terms of B_q^k [eqn. (3)] in the final steps. Additionally, the AOM has served in each step as a constraint on the physical reasonableness of the parameters, such as the basic features of the metal-ligand bond.[14,19] The free-ion F^k and ζ_{5f} parameters, besides the CF parameters, also were varied. As initial values for the free-ion parameters those obtained for $U^{3+} : RbY_2Cl_7$[1] were used. The remaining parameters of the Hamiltonian (2) were fixed at the values characteristic for the U^{3+} ion.[21]

To be more specific, in the initial phase the adjustment of the AOM parameters was performed in three steps. In the first step e_σ was the only parameter freely varied and the values of the others were limited by the following constraints: (a) $e_\pi = 0.5e_\sigma$ and (b) $e_\delta = 0$. The initial value of $e_\sigma = 1000\ cm^{-1}$ as well as the foregoing constraint (a) were obtained from the results of the *ab initio* calculations. In the second step the e_π parameter was varied and its initial value was calculated from relation (a). The initial values of F^k and ζ_{5f} were those obtained from the results for $U^{3+} : RbY_2Cl_7$ as mentioned before. In the next step all three AOM parameters were freely varied with the initial value of $e_\delta = 0$ and those of e_σ, e_π as well as F^k and ζ_{5f} obtained from the second step. The final values of the AOM parameters were $e_\sigma = 1027(\pm 61)\ cm^{-1}$, $e_\pi = 517(+43)\ cm^{-1}$ and $e_\delta = 237(\pm 35)\ cm^{-1}$. During the fitting procedures the AOM parameters were stable and were determined with a relatively small error. Previous AOM results for f-element systems show for chloride ligands the following relationships[14]: $e_\sigma > e_\pi > |e_\delta|$ and $e_\sigma/e_\pi \approx 1.8$–$2.5$. Thus, the empirical values obtained are consistent with expectations.

The next stages of the fitting procedure were performed with the application of the crystal-field parameters B_q^k. The final values of the AOM parameters were used for the determination of the initial values of the B_q^k parameters from the equation:

$$B_q^k = \sum_t \sum_\mu W_{kq}^{\mu t} e_\mu^t \qquad (4)$$

where $W_{kq}^{\mu t}$ are the coefficients determined by the geometry of the coordination polyhedron.

This phase of the calculations was divided into six primary stages, each consisting of a number of steps. They are much more complex than the preceding phases because of the large number of parameters to be determined and the strong correlation between some of them. In each succeeding stage, the initial parameter values were taken as the final values of the earlier one.

In the first stage five second-order crystal-field parameters were simultaneously released and determined. In the second stage the fourth-order crystal-field parameters, with the omission of ReB_3^4 and ImB_4^4 as well as ReB_2^4 and ImB_2^4, also were determined. The crystal-field parameters ReB_3^4 and ImB_4^4 were

Table 2 Free-ion and crystal-field parameters (in cm^{-1}) for U^{+3} (0.3%) : Ba_2YCl_7

Parameter	Fitted value[a] *tab2fnb*	Parameter	Fitted value[a] *tab2fnb*
E_{ave}	19 457 (18)	ImB_3^4	−376 (76)
F^2	39 913 (59)	B_4^4	261 (73)
F^4	33 021 (93)	ImB_4^4	[27][c]
F^6	23 081 (97)	B_0^6	−1084 (94)
α	35,29 (4,5)	B_1^6	496 (77)
β	−1095 (31)	ImB_1^6	[85][c]
γ	1202 (51)	B_2^6	[7][c]
ζ	1617 (7)	ImB_2^6	[33][c]
B_0^2	838 (52)	B_3^6	411 (83)
B_1^2	−250 (51)	ImB_3^6	[37][c]
ImB_1^2	−168 (64)	B_4^6	−753 (65)
B_2^2	−357 (50)	ImB_4^6	171 (89)
ImB_2^2	−363 (53)	B_5^6	−20 (54)[d]
B_0^4	875 (86)	ImB_5^6	−100 (72)[d]
B_1^4	952 (59)	B_6^6	−214 (78)
ImB_1^4	[11][c]	ImB_6^6	−307 (81)
B_2^4	1046 (58)[d]	n^e	65
ImB_2^4	758 (69)[d]	σ^f	25
B_3^4	[27][c]		

[a] The T^i parameters during the fitting procedures were kept at the constant values: $T^2 = 293$, $T^3 = 50$, $T^4 = 183$, $T^6 = -183$, $T^7 = 407$, $T^8 = 300$. The M^j and P^k parameters were constrained by the Hartree–Fock determined fixed ratios: $M^2 = 0.55M^0$, $M^4 = 0.38M^0$, $P^4 = 0.5P^2$, $P^6 = 0.1P^2$. [b] Numbers in parentheses indicate errors in determination of the parameter values. [c] Parameter values in square brackets were kept constant during the fitting procedures at values determined from the AOM adjustment. [d] Separately determined parameters due to strong correlations with the remaining parameters; see section on CF energy level calculations. [e] Number of levels included in the fitting procedure. [f] Deviation: $\sigma = \sum [(\Delta_i)^2/(n-p)]^{1/2}$, where Δ_i is the difference between the observed and calculated energies, n is the number of levels fitted and p is the number of parameters freely varied.

omitted because of their very small values while ReB_2^4 and ImB_2^4 were omitted due to their strong correlation with the remaining parameters. After the determination of all other parameters, the two B_2^4 parameters were varied one-by-one in the fitting procedure. Afterwards, the remaining parameters of fourth order were successively determined with the new values of the B_2^4 parameters fixed. This iteration procedure was repeated until the parameter values became stabilized.

In the third stage the second- and fourth-order parameters, with the exception of ReB_3^4, ImB_4^4 and both B_2^4 were simultaneously varied. Next, similar to the second stage, new values of the B_2^4 parameters were determined separately in subsequent iteration procedures.

In the fourth stage, only the CF parameters of sixth order were first varied. Similarly as in the iteration procedures for the fourth-order parameters in the second stage, the parameters with the smallest values were not taken into account: the ReB_2^6, ImB_1^6 and ReB_3^6 parameters. Since ReB_5^6 and ImB_5^6 were strongly correlated with the remaining parameters, they have been separately determined in a similar way as the B_2^4 parameters in the second stage.

In the fifth stage the parameters of the second, fourth and sixth order were simultaneously varied except for ReB_2^4, ImB_2^4, , ReB_5^6 and ImB_5^6, as well as those mentioned above with very small values. After stabilization of the parameter values in the succeeding iteration procedures the values of B_2^4 (real and imaginary) and B_5^6 (real and imaginary) were separately determined, as in the previous stages.

The last stage of the fitting procedure was similar to that of the fifth one, but at the same time the F^k, ζ_{5f}, α, β and γ free-ion parameters were also varied. In the final step 28 parameters were varied and simultaneously determined, these include eight free-ion parameters. The final stable parameter values are shown in Table 2.

The rms deviation (25 cm^{-1}) and the parameter errors are relatively small. The largest difference between the experimental and calculated CF level values was observed for two components of the $^4F_{9/2}$ multiplet and did not exceed 52 cm^{-1}. From among the determined B_q^k values only those of B_0^6 and the second-order parameters significantly differ from the initial values calculated from the calculated AOM parameters. The relatively large changes in the latter parameter values seem to result from the conventional AOM approach, which does not sufficiently take into account the polarization effects of the U–Cl bonds that mainly influence these values.

The relatively stable nature of the parameter values in all phases of the fitting procedure, as well as the good correspondence between the computed and theoretical parameter values, leads us to conclude that the obtained values retained their physical meaning and that we have avoided in the calculations the pitfall of a local minimum.

A measure of the magnitude of the total crystal-field strength is given by the scalar parameter N_v, defined as[22]

$$N_v = \left[\sum_{k,q} (B_q^k)^2 \frac{4\pi}{(2k+1)}\right]^{1/2} \quad (5)$$

For U^{3+} : Ba_2YCl_7 $N_v = 3154\ cm^{-1}$ and the total splitting of the ground level (Δ) is equal to 538 cm^{-1}. These values correspond well with those determined for U^{3+} in other chloride crystals: U^{3+} : K_2LaCl_5 ($N_v = 3069\ cm^{-1}$, $\Delta = 475\ cm^{-1}$),[2] U^{3+}(site 1) : RbY_2Cl_7 ($N_v = 2823\ cm^{-1}$, $\Delta = 473\ cm^{-1}$)[1] and U^{3+}(site 2) : RbY_2Cl_7 ($N_v = 3505\ cm^{-1}$, $\Delta = 567\ cm^{-1}$).[1]

Conclusion

This paper presents a detailed procedure for calculations of crystal-field parameters of very complex f-electronic systems. The analysis of the obtained high quality low temperature absorption and luminescence spectra permitted the assignment of 65 observed $5f^3 \rightarrow 5f^3$ transitions. The AOM model has been found to be very useful in the determination of the initial B_q^k parameters. It is especially important in all cases where low site symmetries or a small number of available experimental data prevents the application of the B_q^k parametrization procedures. The analysis can be seen as a general method that makes the interpretation of the f-electron spectra of low symmetry systems tractable. Compared with earlier analyses of U(III) systems, the obtained rms errors are among the smallest.

Acknowledgements

M. Karbowiak wishes to thank the Polish – U.S. Fulbright Commission for a Fulbright Research Grant during which a part of this work was completed at Lawrence Berkeley National Laboratory. The work at the Lawrence Berkeley National Laboratory was supported by the Director, Office of Energy Research, Office of Basic Energy Sciences, Chemical Sciences Division of the U.S. Department of Energy under the contract No. DE-ACO3-76SF00098 with the University of California. The Authors wish to thank also Dr Mike Reid (University of Canterbury, New Zealand) for providing his f-shell programs.

References

1 M. Karbowiak, J. Drożdżyński, K. M. Murdoch, N. M. Edelstein and S. Hubert, *J. Chem. Phys.*, 1997, **106**, 3067.

2 M. Karbowiak, N. M. Edelstein, Z. Gajek and J. Drożdżyński, *Spectrochim. Acta A*, 1998, **54**, 2035.
3 M. Karbowiak, J. Drożdżyński, S. Hubert, E. Simoni and W. Stręk, *J. Chem. Phys.*, 1998, **108**, 10181.
4 M. Karbowiak and J. Drożdżyński, *J. Alloys. Compd.*, 2000, **300–301**, 329.
5 M. Karbowiak, Z. Gajek and J. Drożdżyński, *Chem. Phys.*, 2000, **261**, 301.
6 M. Karbowiak, J. Drożdżyński and Z. Gajek, *J. Alloys. Compd.*, 2001, **323–324**, 678.
7 E. Simoni, M. Louis, J. Y. Gesland and S. Hubert, *J. Lumin.*, 1995, **65**, 153.
8 M. S. Wickleder, P. Egger, T. Riedener, N. Furer, H. U. Gudel and J. Hulliger, *Chem. Mater.*, 1996, **8**, 2828.
9 M. Karbowiak and J. Drożdżyński, *J. Alloys. Compd.*, 1998, **271–273**, 836.
10 R. Blachnik and J. E. Alberts, *Z. Anorg. Allg. Chem.*, 1982, **490**, 235.
11 B. G. Wybourne, *Spectroscopic Properties of Rare Earths*, Interscience, New York, 1965.
12 W. T. Carnall, H. Crosswhite, H. M. Crosswhite, J. P. Hessler, N. M. Edelstein, J. G. Conway, G. V. Shalimoff and R. Sarup, *J. Chem. Phys.*, 1980, **72**, 5089.
13 N. M. Edelstein, *J. Alloys Compd.*, 1995, **223**, 197.
14 J. Mulak and Z. Gajek, *The Effective Crystal Field Potential*, Elsevier, Amsterdam, 2000.
15 M. F. Reid, University of Canterburry, New Zealand, private communication.
16 M. Karbowiak, A. Mech, J. Drożdżyński and N. M. Edelstein, *Phys. Rev.*, in press.
17 D. J. Newman, *Adv. Phys.*, 1971, **20**, 197.
18 D. Garcia and M. Faucher, *J. Chem. Phys.*, 1985, **82**, 5554.
19 Z. Gajek and J. Mulak, *J. Phys.: Condens. Matter*, 1992, **4**, 427.
20 Z. Gajek, *J. Alloys. Compd.*, 1995, **219**, 238.
21 W. T. Carnall, *A Systematic Analysis of Trivalent Actinides Chlorides in D_{3h} Site Symmetry*, in ANL Report 89/39, Argonne National Laboratory, Nov. 1989, pp. 1–285 (National Techn. Infor. Service, Springfield, VA, 22161).
22 F. Auzel and O. L. Malta, *J. Phys.*, 1983, **44**, 201.